ARCHIVES OF CIVIL AND MECHANICAL ENGINEERING 14 (2014) 170–180

Available online at www.sciencedirect.com

SciVerse ScienceDirect

journal homepage: www.elsevier.com/locate/acme

Original Research Article

Calibration of concrete parameters based on digital image correlation and inverse analysis

*T. Gajewski, T. Garbowski**

Poznan University of Technology, Institute of Structural Engineering, ul. Piotrowo 5, 60-965 Poznan, Poland

ARTICLE INFO

Article history:
Received 6 April 2013
Accepted 30 May 2013
Available online 11 June 2013

Keywords:
Lubliner model
Digital image correlation
Inverse analysis

ABSTRACT

The main goal of this paper is to present a robust calibration procedure of essential material parameters of concrete models, based on both full-field measurements and inverse analysis. The proposed method uses a simple laboratory test and home-made correlation software alongside a fast camera. Usually, a full set of material model parameters of concrete can be determined through application of several different tests and specimen conditions. A recent method requires just one test for identification of most of the model constants. It reduces the time needed for testing and provides a relatively fast calibration of the selected parameters through minimization of discrepancies both of experimentally measured displacement fields on the specimen surface and of the numerically computed corresponding quantities. A study of an efficient correlation algorithm and of a reliable minimization gradient-based algorithm is also presented.

1. Introduction

Concrete has a wide application in civil engineering, being used as a typical construction material for modern buildings, structure foundations, arch-gravity dams and soil stabilization systems, to list just a few. Often, engineers need to design or analyze concrete structures, working not only in the linear elastic range but also far beyond that. Such advanced analyses require appropriate constitutive modeling of the material in order to capture its main characteristic and behavior. Constitutive modeling of concrete has attracted a lot of attention in many research fields in the last decades. Researchers have developed a wide variety of models in an attempt to capture and mathematically describe many important features of concrete. Unfortunately, due to the heterogeneous nature of such material, there is no single model capable of mimicking all of its characteristics, therefore great care needs to be taken in the selection of an appropriate material model that has been designed to emulate expected behavior.

Concrete is a composite pressure-sensitive material with a dramatically lower tensile strength than compressive strength. An analysis of a structure that is majorly subjected to tensile loading (which typically leads to the formation and propagation of cracks normal to the axis of maximum principal stress) will probably be done using the simple Rankine criterion [28], which can reasonably well describe such a failure mode. Alternatively, if respectively greater compressive loads are expected, the Drucker–Prager criterion in its original form [7] or enhanced with a cap yield surface [29] would be more suitable choice. For structures both under tension and compression loading criteria which combine these two models might be selected [8,11].

*Corresponding author. Tel.: +48 616652099.
E-mail addresses: tomasz.gajewski@put.poznan.pl (T. Gajewski), tomasz.garbowski@put.poznan.pl (T. Garbowski).

1644-9665/$ - see front matter © 2013 Politechnika Wrocławska. Published by Elsevier Urban & Partner Sp. z o.o. All rights reserved.
http://dx.doi.org/10.1016/j.acme.2013.05.012

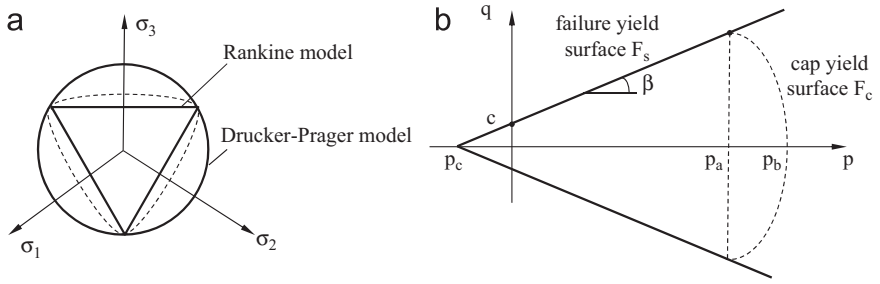

Fig. 1 – Typical yield surfaces of deviatoric sections for: (a) both the Rankine and the Drucker–Prager model and (b) the Drucker–Prager model alone with a cap in the meridian plane.

Typically, experimental results for concrete tend to indicate that the strength envelope (failure surface) within principal stress space is a deformed cone with three planes of symmetry, which all intersect at the hydrostatic axis. The deviatoric sections (octahedral plane projections) take the form of rounded triangles whose shapes vary from almost triangular with tensile and low compressive hydrostatic pressures to almost circular with high compressive hydrostatic pressures (see Fig. 1a). Triangularly shaped deviatoric sections correspond to the Rankine criterion and circularly shaped sections correspond to the Drucker–Prager criterion. Such variations in the deviatoric section's shape can also be described in terms of the so-called meridians, i.e. intersections of the failure surface with the half-planes that begin at the hydrostatic axis (see Fig. 1b). Such variations in the meridians of deviatoric sections usually have exponential, hyperbolic or linear relations, depending on the failure criteria [1,18,26,27].

Additionally the tensile cracking or compressive crushing of concrete usually leads to a degradation in its elastic stiffness, which is not reflected by the standard plasticity models that unload with an initial slope. Stiffness degradation can be handled within the framework of fracture mechanics or damage mechanics (using a proper localization limiter). The so-called smeared crack models [31], popular in engineering applications, can be interpreted as a special type of damage model [4,17]. However, provided that the energy dissipation caused by localized fracture and the existence of a characteristic length are properly taken into account, the cracking of concrete under monotonic loading can also be approximated using a model based exclusively on the theory of plasticity.

A group of constitutive models that suitably describes these complex phenomena is based on a combination of the flow theory of plasticity and damage mechanics. Plasticity models alone [5,6,8,19,23] are unable to capture the stiffness degradation that has been observed in experiments. On the other hand, damage models are unsuitable for describing both the irreversible deformations and inelastic volumetric expansion that occur during compression. Combinations of plasticity models and damage models [14–16,21] usually consider plasticity with isotropic hardening and enrich it with either isotropic or anisotropic damage.

The problem of selecting a proper material model suitable for this specific kind of numerical analysis is complicated further when taking into consideration another aspect, which is how difficult the model is to calibrate. A compromise would be to use a model that reasonably reflects the main features of the material and has a relatively easy calibration procedure. However, the more sophisticated the model is, the more parameters there are to identify and the more complicated the tests are. Using a simpler model, which thus has smaller set of parameters to characterize, one can attempt to design a simple and straightforward experiment, which could possibly be enhanced by new measurement techniques that help to extract more information from the test. A number of modern techniques that enrich the standard tests can be applied, using equipment that is available on today's market (e.g. thermal imaging, vibrations registration, body motion tracking and waveguide sensors). Among these techniques is digital image correlation (DIC), which belongs to a group of visual non-contacting methods that track the deformation or motion of recorded objects [30]. DIC is often used as a measurement tool within an inverse procedure for the characterization of material properties (cf. e.g. [9,10,12]). This primarily is because a certain amount of information taken from such measurements helps, not only to regularize the inverse problem but also to extend the number of possible to identify parameters from a single test.

2. Experimental setup

The proposed procedure is based on a simple compression uniaxial test of a normalized cubic concrete specimen. The compression test is performed under standard conditions, e.g. with the specimen compressed on top of a rigid base the quasi-static loading velocity ranging from 0.2 to 1.0 MPa/s, and the strain rate not exceeding 10^{-6} 1/s.

The experiment is carried out on an Instron 8500 (http://www.instron.tm.fr) four-column frame servohydraulic fatigue testing machine with compressive force capacities of up to 1000 kN (see Fig. 2a). These electronically controlled and versatile systems can perform static, fatigue and dynamic tests on various materials.

From the experimental data (i.e. experimental curve) resulting from a standard displacement-controlled test, one can determine the elastic modulus E, the compressive strength σ_c, possibly the crushing energy G and the stiffness degradation d so long as cycling loading is applied (see Fig. 3). However, our goal is to determine more parameters (without involving other experiments). Therefore the standard compression test must be improved through additional experimental techniques. Here, non-contacting full-field measurements of displacements on

the side surface of the specimen are taken so as to enrich the experimental data. The deformation field recorded by the camera is fully calibrated with an applied load or displacement, so the corresponding field of displacements can be determined during each stage of the experiment. This makes it possible to build a test simulation in which all experimental conditions can be reconstructed. The only unknown parameters of the numerical model are the materials' constants. Therefore by applying an inverse analysis, an initial guess of the unknown parameters can be made and iteratively improved on through minimization of the discrepancy between the numerically computed measurable quantities and the experimentally measured ones.

2.1. *DIC equipment and correlation algorithms*

Digital image correlation is a technique developed for the determination of displacements and strains, based on the acquisition and comparison of relevant digitized pictures. The experimental equipment used to acquire digital images in this work is displayed in Fig. 2b. The system uses the high-speed Phantom v711 camera (http://www.visionresearch.com/Products/High-Speed-Cameras/v711) at a resolution 800×800 pixels.

The accuracy of measurements for a given image resolution and monitored area size can be easily estimated using the empirical formula h/w, where h is a pixel size and w is either 10 or even 100 depending on the selected correlation algorithm. Producers of the DIC systems suggest to compute the accuracy using the formula

$$\text{accuracy} = \frac{\text{max picture length}}{100.000}. \tag{1}$$

In practice, the denominator in Eq. (1) should rather be one order of magnitude lower. Here, a front-facing surface of a concrete specimen has been recorded as pictures of a size of approximately 100×100 mm. According to the aforementioned practical outline, the accuracy of such measurements will be either 1 or 10 μm. Consequently, the smallest change in displacement that can be caught on digital camera is equal to either 1 or 10 μm. This accuracy directly affects the requirements of a DIC measurement system. Therefore, the displacements between two correlated images should be large enough to allow for recordable measurements error. This restricts the number of images which can be used in a DIC setup.

In the case of a compressive uniaxial test of a specimen of 100 mm in height, the recorded displacements can be lower than the assumed accuracy of DIC system. Fig. 4 demonstrates such cases for the x-direction displacement (a) (applied to 50% of the total displacement U) and (b) for y-displacement (applied to 10% of total displacement U), where a lighter color represents a region where the displacement is lower than the accuracy and a darker color indicates a region where the displacement is greater then an accuracy of 10 μm. Therefore only darker color regions can be taken into consideration during DIC procedure.

The acquired grayscale photographs are recorded in digitized form, so each pixel represents a number, which ranges from 0 to 255. The lowest value represents black, the highest value white, numbers in between correspond to different shades of gray. Digital image correlation therefore becomes a

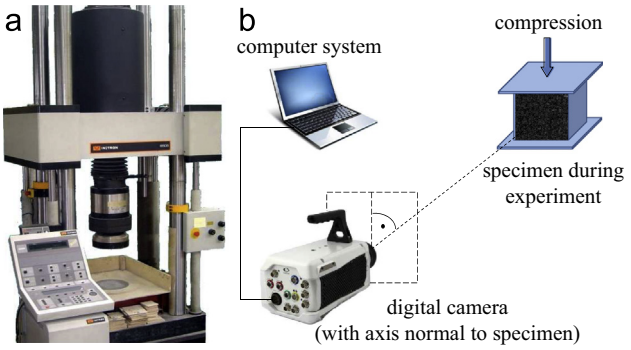

Fig. 2 – (a) Instron 8500 testing machine and (b) image acquisition system.

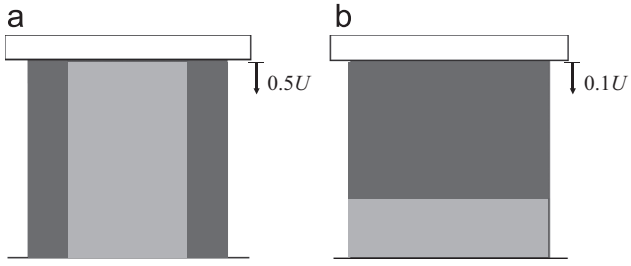

Fig. 4 – Acquisition fields of displacements captured by a DIC system: (a) in the x-direction and (b) in the y-direction.

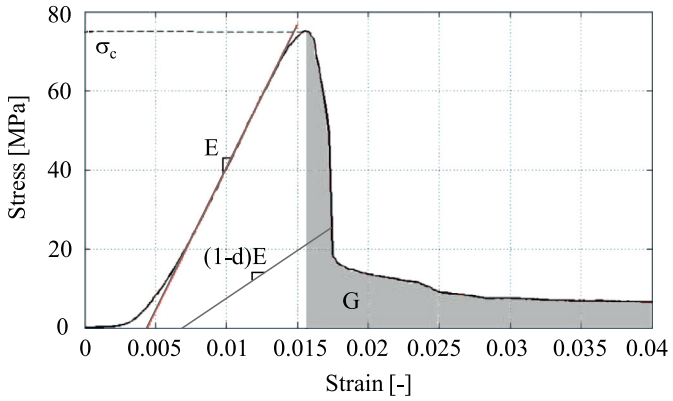

Fig. 3 – Experimental curve of concrete from a compression displacement-controlled test.

task of comparing two subsets of numbers of two digital images. A typical function, which measures how well two subsets match to each other, is

$$S\left(x, y, u, v, \frac{\partial u}{\partial x}, \frac{\partial u}{\partial y}, \frac{\partial v}{\partial x}, \frac{\partial v}{\partial y}\right) = 1 - C_i(f(x,y), g(x',y')) \tag{2}$$

where $C(\cdot)$ is a correlation function that gives a value of one if a full correlation is achieved, $f(x,y)$ is the gray level pixel-value at coordinate (x,y) of the reference image and $g(x',y')$ is the gray level pixel-value at point (x',y') of the second image of the deformed specimen. The coordinates (x,y) and (x',y') are related by the deformation which has occurred in the time between the acquisition of the two images.

If the motion of the object relative to the camera is parallel to the image plane, then the coordinates are given by

$$x' = x + u + \frac{\partial u}{\partial x}\Delta x + \frac{\partial u}{\partial y}\Delta y \tag{3}$$

$$y' = y + v + \frac{\partial v}{\partial x}\Delta x + \frac{\partial v}{\partial y}\Delta y \tag{4}$$

where u and v are the displacements of the subset centers in the x- and y-directions, respectively. The terms Δx and Δy are the distances from the subset center to point (x,y). All unknown values u, v, $\partial u/\partial x$, $\partial u/\partial y$, $\partial v/\partial x$, and $\partial v/\partial y$ gathered in a vector $\mathbf{p}$ can be found by minimizing the correlation coefficient S.

Correlation criteria are usually classified into two common families, namely those of cross-correlation (CC) and sum-squared difference (SSD) correlation. The typical correlation functions used for the evaluation of the similarity between the reference and the deformed subset have been gathered into Tables 1 and 2, see [25].

In the formulas presented in the tables the mean value of pixel shade intensity within a single reference subset of the undeformed picture f_m is calculated using the formula

$$f_m = \frac{1}{(2M+1)^2}\sum_{i=-M}^{M}\sum_{j=-M}^{M} f(x_i, y_i) \tag{5}$$

and in the corresponding reference subset of the deformed picture using

$$g_m = \frac{1}{(2M+1)^2}\sum_{i=-M}^{M}\sum_{j=-M}^{M} g(x'_i, y'_i). \tag{6}$$

The norms of the reference subsets in the undeformed and the deformed pictures are computed respectively using

$$\overline{f} = \sqrt{\sum_{i=-M}^{M}\sum_{j=-M}^{M}[f(x_i, y_i)]^2}, \tag{7}$$

$$\overline{g} = \sqrt{\sum_{i=-M}^{M}\sum_{j=-M}^{M}[g(x'_i, y'_i)]^2}. \tag{8}$$

The normalized norms of the reference subsets in the undeformed and the deformed pictures are computed using the corresponding formulas

$$\Delta f = \sqrt{\sum_{i=-M}^{M}\sum_{j=-M}^{M}[f(x_i, y_i) - f_m]^2}, \tag{9}$$

$$\Delta g = \sqrt{\sum_{i=-M}^{M}\sum_{j=-M}^{M}[g(x'_i, y'_i) - g_m]^2}, \tag{10}$$

where M is the distance in pixels from the center of the reference subset to the furthest pixel in either the horizontal or vertical direction.

It can be proved that the CC and SSD criteria families are directly related, e.g. ZNCC criterion can be easily derived from the ZNSSD correlation criterion, namely $C_{ZNSSD}(\mathbf{p}) = 2[1 - C_{ZNCC}(\mathbf{p})]$. Similarly, the other criteria can each be computed from each other. Moreover, it is worth noting that if the intensity values of the gray pixels on a certain image are transformed using the linear function $g'(x',y') = a \times g(x',y') + b$ (see e.g. [25]), the values of the ZNCC and ZNSSD correlation criteria will not change. Therefore the ZNCC and ZNSSD correlation criteria serve as an extremely robust noise-proof correlation tool, which is insensitive to offsets and linear changes in illumination lighting. Correspondingly, although the NCC and NSSD correlation criteria do not appear to be sensitive to linear changes in illumination lighting, they are sensitive to offsets in lighting. The least robust performances are shown by those that use CC and SSD correlation criteria, which are sensitive to all variations in lighting.

DIC picture acquisition. The 2D DIC method requires the following steps to be performed: (1) specimen and experimental preparations; (2) the recording of images of the planar specimen surface before and after loading; (3) the processing of the acquired images using a computer system in order to obtain the desired displacement and strain information.

In order to uniquely identify the position of small sets of pixels the specimen surface must have a random gray intensity distribution (i.e. a random speckle pattern), which will deform with the specimen surface. For details on this, see [30]. The speckle pattern can be formed using the natural texture of the specimen surfaces, constructed artificially through the spraying of black and/or white paints, or using other techniques. It is important for the camera to be placed

Table 1 – Commonly used cross-correlation criterion: cross-correlation (CC), normalized cross-correlation (NCC), zero-normalized cross-correlation (ZNCC).

$$C_{CC} = \sum_{i=-M}^{M}\sum_{j=-M}^{M}[f(x_i, y_j)g(x'_i, y'_j)]$$

$$C_{NCC} = \sum_{i=-M}^{M}\sum_{j=-M}^{M}\left[\frac{f(x_i, y_j)g(x'_i, y'_j)}{\overline{f}\,\overline{g}}\right]$$

$$C_{ZNCC} = \sum_{i=-M}^{M}\sum_{j=-M}^{M}\left[\frac{[f(x_i, y_j) - f_m] \times [g(x'_i, y'_j) - g_m]}{\Delta f \Delta g}\right]$$

Table 2 – Commonly used sum-squared difference criterion: sum-squared difference (SSD), normalized sum-squared difference (NSSD), zero-normalized sum-squared difference (ZNSSD).

$$C_{SSD} = \sum_{i=-M}^{M}\sum_{j=-M}^{M}[f(x_i, y_j) - g(x'_i, y'_j)]^2$$

$$C_{NSSD} = \sum_{i=-M}^{M}\sum_{j=-M}^{M}\left[\frac{f(x_i, y_j)}{\overline{f}} - \frac{g(x'_i, y'_j)}{\overline{g}}\right]^2$$

$$C_{ZNSSD} = \sum_{i=-M}^{M}\sum_{j=-M}^{M}\left[\frac{f(x_i, y_j) - f_m}{\Delta f} - \frac{g(x'_i, y'_j) - g_m}{\Delta g}\right]^2$$

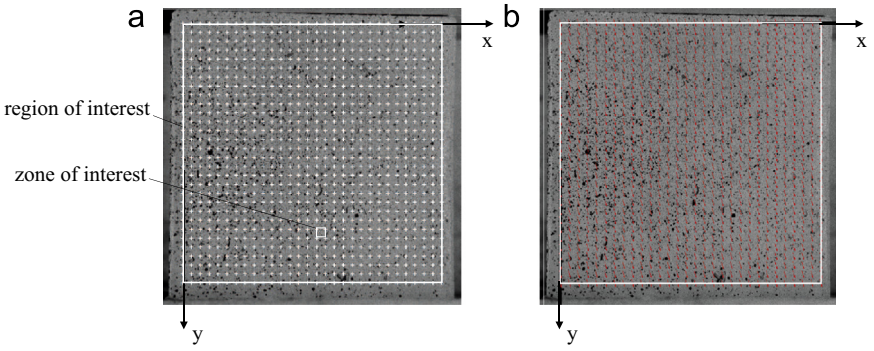

Fig. 5 – Example of (a) ROI and grid of ZOI and (b) the red displacement vectors, calculated in the centers of the ZOI and presented on the deformed image.

with its optical axis normal to the specimen surface, hence projecting the planar specimen surface in different loading states onto its sensor plate (see Fig. 2b).

In a routine implementation of the 2D DIC method, the calculation area (i.e. region of interest or ROI) of the reference image should be specified or defined at first, which is then further divided into evenly spaced virtual image points (zones of interests or ZOIs) as shown in Fig. 5a. Displacements are computed at each point on the virtual grid to obtain the full-field deformation (see e.g. [25,30]). The main idea of 2D DIC, as has been mentioned already, is to record two images before and after deformation and then to track deformation of the same points (or pixels) between them. This is shown schematically in Fig. 6. In order to compute the displacements of a point P, a square reference subset of $(2M+1)\times(2M+1)$ pixels centered at point $P(x,y)$ in the reference image is selected so it can be used to track the point's corresponding location in the deformed image. A square subset, rather than an individual pixel, is selected for matching since a subset with a wider variety of gray levels of pixels can be more easily distinguished from other subsets. Therefore each deformation can be more easily identified within the image.

Correlation algorithms. In this study, a professional camera was used with no built-in software. Therefore the correlation algorithm was implemented in an attempt to compute displacements from a series of images. Herein two recognized and widely used algorithms were implemented as Matlab [22] subroutines. These were later checked for accuracy, correlation time and robustness, and then compared against each other.

Firstly, a coarse-fine search technique was employed to study image correlation. The algorithm checked many possible variable combinations within a given range and compared the correlation factors for each set. Since a large number of calculations was required, this technique was usually only applied to determine the values of u and v.

Due to the discrete nature of the digitized image, no gray level information was available for the space between the pixels. If only pixel center coordinates were used for x, y in Eq. (2), the displacements and gradient terms would not be independent. Therefore, the gray pixel-level values of the space between the pixels needed to be approximated.

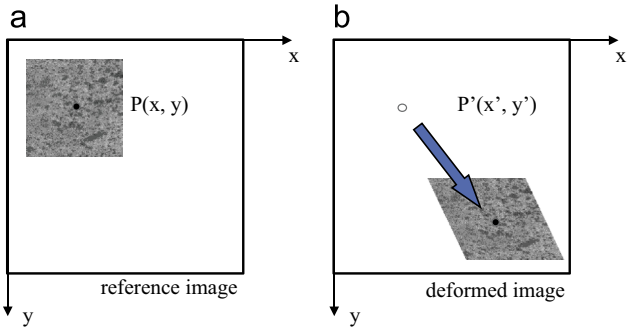

Fig. 6 – Schematic illustration of a square subset: (a) before deformation (reference) and (b) after deformation.

For the coarse-fine search method, bilinear interpolation is often used. Such interpolation approximates the gray level value at a point (x',y'), which is between the pixels (i,j), $(i+1,j)$, $(i,j+1)$ and $(i+1,j+1)$, by the formula

$$g(x',y') = a_{00} + a_{10}(\Delta x) + a_{01}(\Delta y) + a_{11}(\Delta x)(\Delta y) \tag{11}$$

where a_{00} is a gray level value of pixel (i,j), a_{10} is a gray level value of pixel $(i+1,j)$–a_{00}, $a_{01}$is a gray level value of pixel $(i,j+1)$–a_{00} and $a_{11}$is a gray level of pixel $(i+1,j+1)$–a_{00}–a_{10}–a_{01}. Δx and Δy are the x and y distances from pixel (i,j). If one would like to obtain a higher accuracy, bicubic spline interpolation can be used. The functional form for the gray level value at (x',y'), which is between pixels (i,j), $(i+1,j)$, $(i,j+1)$, and $(i+1,j+1)$, and uses a bicubic spline

$$g(x',y') = \sum_{i=0}^{3}\sum_{j=0}^{3} a_{ij}\Delta x^i \Delta y^j \tag{12}$$

where a_{ij} are the coefficients which can be calculated based on given boundary conditions using the f function values. Its first order derivatives f_x, f_y and cross derivative f_{xy} exist at nodal locations. The coefficients must adhere to the condition that all first order and cross derivatives are continuous between adjacent surfaces, see [2].

An alternative to the aforementioned is the Newton–Raphson method, which is capable of finding the six deformation parameters that can be applied to minimize the correlation function (2), which are u, v, $\partial u/\partial x$, $\partial u/\partial xy$, $\partial v/\partial x$, and $\partial v/\partial y$. This technique allows these parameters to be determined with less computational processing than the

previous coarse-fine search method. The Newton–Raphson method is based on the calculation of correction terms, which improve on previously determined initial guesses. The correction for a single estimate i is given by

$$\Delta\mathbf{p} = -H^{-1}(\mathbf{p})\nabla(\mathbf{p}) \tag{13}$$

where $\mathbf{p}$ is equivalent to $[u, v, \partial u/\partial x, \partial u/\partial y, \partial v/\partial x, \partial v/\partial y]^T$ and $\nabla(\mathbf{p})$ is the Jacobian matrix. Each element of the Jacobian matrix is a derivative of the correlation function evaluated for a guess i. The Jacobian matrix is as follows:

$$\nabla(\mathbf{p}) = \frac{\partial S}{\partial p_i}, \tag{14}$$

$H(\mathbf{p}_i)$ is the Hessian matrix, which is the second partial derivative of the correlation function

$$H(\mathbf{p}) = \frac{\partial^2 S}{\partial p_i \partial p_j}. \tag{15}$$

The Newton–Raphson algorithm (NRA) must first obtain an initial estimate of the deformation parameters $\mathbf{p}$, which are later added to the initial guess and the process is iterated until convergence is obtained. This algorithm requires the starting guess to be relatively close to the required solution, hence requiring an additional method of starting point selection. This can be easily done by performing a correlation of the four corners of the ROI (see Fig. 5) using a course-fine algorithm (CFA) on the pixel level. By linear (shape) interpolation of the calculated estimates one can guarantee decent starting points for the subsequent ZOI regions' correlation so long as the deformations are continuous within the ROI.

In order to compare the performance of the two previously discussed algorithms, a simple example of the correlation of a single square 101 × 101 region (see Fig. 7a) from a ROI drawn on a sample surface (see Fig. 5) is presented here. In Fig. 7c the converged solution on a reduced size ZOI consisting of 21 × 21 pixels is shown. The result was obtained using a two-step procedure: firstly, the course-fine approximation was found and secondly, the Newton–Raphson method was employed. In Fig. 7b the reference ZOI is shown, whereas in Fig. 7d deformed ZOI is depicted.

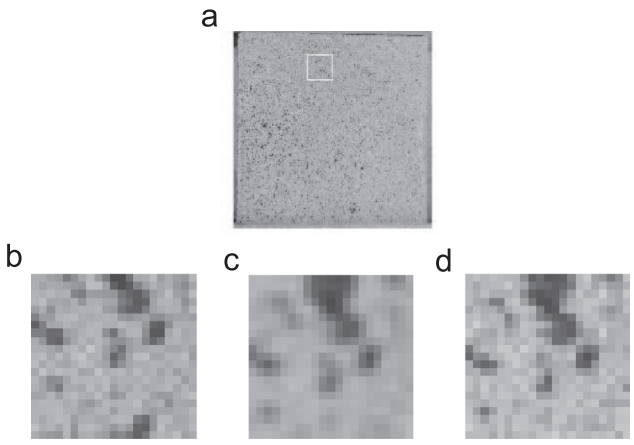

Fig. 7 – A ZOI selected from (a) the ROI (i.e. the white square), (b) a reference ZOI position, (c) the converged position of reduced ZOI, and (d) the position of ZOI in the deformed configuration.

The performance of both CFA with bicubic interpolation and NRA is presented in Table 3. It is clear from the above comparison that NRA performs much better then CFA with bicubic interpolation for two reasons: (1) it provides more information in a shorter time and (2) it gives more accurate results in terms of ZOI center position.

2.2. *Inverse analysis and minimization algorithm*

Once the displacement field for discrete points on the specimen surface is computed via the selected correlation algorithms and with sufficient accuracy, one can start to simulate an experimental test. In order to do this, the following features of the numerical model need to be ascertained: (a) the description of geometry, (b) the boundary conditions, (c) the initial conditions, and (d) the properties of all of the involved materials (i.e. the constitutive constants). From this list, three factors are directly dependent on the experimental setup. The only unknowns are therefore the materials' parameters. By using an initial guess of the model constants, which could, for example, be gathered using expert knowledge or literature, a solution a reasonably accurate can be made. From this point on, through iteratively employing inverse analysis, the unknown material parameters can be identified.

The inverse analysis (also known as back-calculation analysis) method merges the numerically computed $\mathbf{U}_{NUM}$ and experimentally determined $\mathbf{U}_{EXP}$ measurable quantities for discrepancy minimization. A vector of residua $\mathbf{R}$ can be constructed in the following way:

$$\mathbf{R} = \mathbf{U}_{EXP} - \mathbf{U}_{NUM}(\mathbf{x}). \tag{16}$$

This measures the differences between the aforementioned measurable quantities. By adjusting the constitutive parameters (encapsulated in the vector $\mathbf{x}$) embedded in the numerical model, which in turn mimic the experimental setup, an iterative convergence towards the required solution can be achieved. The minimization of the objective function ω (within the least square frame) takes the form

$$\omega = \sum_{i=1}^{n} (R_i)^2 = \|\mathbf{R}\|_2^2 \tag{17}$$

and is usually updated through the use of first-order (gradient-based) or zero-order (gradient-less) algorithms. Procedures based on a soft method (e.g. genetic algorithms, simulated annealing,

Table 3 – ZOI's pixel displacement and deformation computed using both CFA with bicubic interpolation and NRA.

Algorithm	u	v	$\partial u/\partial x$	$\partial u/\partial y$	$\partial v/\partial x$	$\partial v/\partial y$
CFA + bicubic interpolation	−0.258	−3.90	–	–	–	–
NRA	−0.571	−3.51	0.0016	0.0016	0.0051	−0.0078

particle swarm algorithms) can be also used for function minimization, especially when the function is non-convex and so has many local minima. However, such algorithms usually require many iterations. Among the many first-order procedures that are based on either the Gauss–Newton or the steepest descent direction in a nonlinear least square methods, the trust region algorithm (TRA) seems the most effective. The TRA uses a simple idea, similar to that in Levenberg–Marquardt (LM) algorithm (see e.g. [24]), which performs each new step in a direction combining the Gauss–Newton and steepest descent directions. The LM algorithm computes new directions using the following formula:

$$\Delta\mathbf{x} = -(\mathbf{H}_\mathbf{x} + \lambda\mathbf{I})^{-1}\mathbf{g}_\mathbf{x} \tag{18}$$

where λ is an internal parameter, $\mathbf{g}_\mathbf{x} = \nabla\omega(\mathbf{x})$ is the gradient of the objective function ω with respect to the parameters $\mathbf{x}$

$$\mathbf{g}_\mathbf{x} = \frac{\partial\omega}{\partial\mathbf{x}}, \tag{19}$$

and the Hessian $\mathbf{H}_\mathbf{x} = \nabla^2\omega(\mathbf{x})$ is a second partial derivative of ω with respect to the parameters $\mathbf{x}$

$$\mathbf{H}_\mathbf{x} = \frac{\partial^2\omega}{\partial\mathbf{x}^2}, \tag{20}$$

In the nonlinear least square approach method, the gradient and Hessian matrix can be computed using the Jacobian matrix

$$\mathbf{J}(\mathbf{x}) = \frac{\partial\mathbf{R}}{\partial\mathbf{x}} \tag{21}$$

so the gradient and Hessian matrix are defined, respectively

$$\mathbf{g}(\mathbf{x}) = \mathbf{J}^T\mathbf{R}, \quad \mathbf{H}(\mathbf{x}) \simeq \mathbf{J}^T\mathbf{J}. \tag{22}$$

Such approximation of the Hessian, which can be computed 'for free' once the Jacobian is available, represents a distinctive feature of least squares problems. This approximation is valid if the residuals are small, meaning we are close to the solution. Therefore some techniques may be required in order to ensure that the Hessian matrix is semi-positive defined (see e.g. [24]).

One of the main issues of the trust region approach, which to a large extent determines the success and the performance of this algorithm, is in deciding how large the trusted region should be. Allowing it to be too large can cause the algorithm to face the same problem as the classical Newton direction line search, when the model function minimizer is quite distinct from the minimizer of the actual objective function. On the other hand using too small a region means that the algorithm will miss the opportunity to take a step substantial enough to move it much closer to the solution.

Each k-th step in the trust region algorithm is obtained by solving the sub-problem defined by

$$\min_{\mathbf{d}_k} m_k(\mathbf{d}_k) = f(\mathbf{x}_k) + \mathbf{d}_k^T\nabla f(\mathbf{x}_k) + \frac{1}{2}\mathbf{d}_k^T\nabla^2 f(\mathbf{x}_k)\mathbf{d}_k, \quad \|\mathbf{d}_k\| \le \Delta_k \tag{23}$$

where Δ_k is the trust region radius. By writing the unknown direction as a linear combination of Newton and steepest descent direction, the sub-problem will take the following form:

$$\begin{aligned}\min m_k(\mathbf{x}_k) = f(\mathbf{x}_k) &+ [s_1\mathbf{d}_k^{SD} + s_2\mathbf{d}_k^N]^T\nabla f(\mathbf{x}_k) \\ &+ \tfrac{1}{2}[s_1\mathbf{d}_k^{SD} + s_2\mathbf{d}_k^N]^T\nabla^2 f(\mathbf{p}_k)[s_1\mathbf{d}_k^{SD} + s_2\mathbf{d}_k^N]\end{aligned} \tag{24}$$

under the constrains

$$\|s_1\mathbf{d}_k^{SD} + s_2\mathbf{d}_k^N\| \le \Delta_k. \tag{25}$$

The problem now becomes two-dimensional and it is solved for the unknown coefficients s_1 and s_2. In order to find both s_1 and s_2 in Eq. (25) a set of nonlinear equations can be solved using, for example, the Newton–Raphson techniques that were mentioned in the previous section. Herein this approach is implemented using an inverse procedure to compute the discrepancy minimization between the displacement measured by DIC and the corresponding ones computed by the numerical model. The numerical model thus still requires a constitutive model to be selected and tuned using inverse analysis.

2.3. *Selected constitutive model of concrete*

In this work, the Lubliner type of constitutive model is used (see [20]). The model can capture most of the characteristics of concrete, keeping the number of parameters at a reasonable practical level (see [13,32,33]). The Lubliner yield criterion takes the form

$$\frac{1}{1-\alpha}(\sqrt{3J_2} + \alpha I_1 + \beta\langle\sigma_{max}\rangle - \gamma\langle-\sigma_{max}\rangle) = c, \tag{26}$$

where α, β and γ are dimensionless constants to be calibrated by the experiments, J_2 is the second invariant of the deviatoric stress tensor, I_1 is the first invariant of the stress tensor, σ_{max} is the maximum principal stress, c is the compressive cohesion and the Macaulay brackets $\langle\cdot\rangle$ are defined as $\langle x\rangle = (|x| + x)/2$.

It is noted here that Eq. (26) is actually a form of the yield criterion after being calibrated using uniaxial compression, from which the original form can be derived as

$$\sqrt{3J_2} + \alpha I_1 + \beta\langle\sigma_{max}\rangle - \gamma\langle-\sigma_{max}\rangle - \delta c = 0, \tag{27}$$

where δ is a fourth dimensionless constant. When concrete yields during uniaxial compression, $J_2 = c^2/3$, $I_1 = c$, and $\sigma_{max} = 0$. Substituting these into (27), we get $\delta = 1-\alpha$, and the original form in (27) becomes the commonly used form in (26).

The form of the Lubliner yield criterion depends on the sign of the maximum principal stress σ_{max}. We can distinguish between three possible scenarios:

(1) $\sigma_{max} > 0$, i.e. tensile stress is present, so (26) reduces to

$$\frac{1}{1-\alpha}(\sqrt{3J_2} + \alpha I_1 + \beta\sigma_{max}) = c, \tag{28}$$

(2) $\sigma_{max} = 0$, for uniaxial or biaxial compression, so (26) reduces to

$$\frac{1}{1-\alpha}(\sqrt{3J_2} + \alpha I_1) = c \tag{29}$$

(3) $\sigma_{max} < 0$, for triaxial compression, so (26) reduces to

$$\frac{1}{1-\alpha}(\sqrt{3J_2} + \alpha I_1 + \gamma\sigma_{max}) = c. \tag{30}$$

Eq. (28) can be regarded as a combination of the Drucker–Prager criterion, which describes shear failure mechanisms, and the Rankine criterion, which describes tensile failure

mechanisms. While (30) can be regarded as a modification of the Drucker–Prager criterion which accounts for the changes in the deviatoric sections (see Fig. 1a).

Usually, the parameter α is calibrated from Eq. (29) through use of the uniaxial compressive strength f_c and the equibiaxial compressive strength f_{bc} as

$$\alpha = \frac{f_{bc}/f_c - 1}{2f_{bc}/f_c - 1}, \tag{31}$$

and then the parameter β is calibrated from (28) using the uniaxial compressive strength f_c and the uniaxial tensile strength f_t as

$$\beta = (1-\alpha)f_c/f_t - (1+\alpha). \tag{32}$$

The parameter γ is calibrated from (30) by making use of the ratio K_c between $\sqrt{J_2}$ on the tensile meridian and that on the compressive meridian at a given hydrostatic pressure in triaxial compression as [33,32]

$$\gamma = \frac{3(1-K_c)}{2K_c - 1} \tag{33}$$

The plastic flow rule of a material model of concrete usually assumes a non-associative potential flow, meaning the increment of plastic deformations is normal to a plastic flow function rather than to a yield function. The inelastic deformation increment is, therefore, computed as follows:

$$\dot{\boldsymbol{\varepsilon}}^{pl} = \frac{\partial G}{\partial \boldsymbol{\sigma}} \tag{34}$$

The flow potential of the Lubliner model implemented here is the Drucker–Prager linear function

$$G = t - p\ \tan\ \psi, \tag{35}$$

where

$$t = \frac{1}{2}q\left[1 + \frac{1}{K_c} - \left(1 - \frac{1}{K_c}\right)\left(\frac{r}{q}\right)^2\right],$$

$$q = \sqrt{\tfrac{3}{2}\mathbf{s} : \mathbf{s}}, \quad r = \sqrt{\tfrac{9}{2}\mathbf{s} \cdot \mathbf{s} : \mathbf{s}}, \quad p = \tfrac{1}{3}\mathrm{tr}(\boldsymbol{\sigma}),$$

ψ is a dilation angle in the p–t plane and $\mathbf{s}$ is a stress deviator.

Therefore the set of parameters in the selected elasto-plastic material model of concrete can be listed as: E—Young's modulus, ν—Poisson's ratio, ψ—the dilation angle, K_c—the ratio between deviator in tensile meridian and in compressive meridian, f_c—the compressive strength, f_t—the tensile strength, and f_b—the equibiaxial compressive strength.

3. Results

The selected results of the study on characterization of concrete material constants are presented in this section. As specified in previous sections, the following tools and procedures are used in this study: (1) a simple uniaxial test performed on a Instron 8500, (2) the DIC equipment, namely the digital camera Phantom v711 and the Newton–Raphson correlation algorithm, (3) an inverse procedure based on the least square approach and an iterative TRA and (4) a finite element (FE) numerical model for test simulation with an implemented Lubliner-type material model of concrete specimens.

Table 4 – Reference values of parameters used for sensitivity and inverse calculations.

Parameter	Value
E (GPa)	30
Ψ (°)	38
K_c (–)	0.667
σ_c (MPa)	45
σ_t (MPa)	4.5
H (GPa)	0.2
f_b/f_c (–)	1.16

The test simulation is performed here by making use of the FE model, which is constructed with a quarter of the geometry of an analyzed sample and is discretized using 4960 linear hexahedral elements with mean size of 0.004 m. Additional, intrinsic boundary conditions are applied so as to double symmetry of structure. An implementation of the Lubliner-type material model in Abaqus is used with parameters specified as in the previous section (the reference parameters are shown in Table 4). In order to simplify the identification procedure of the following numerical examples the Poisson's ratio is assumed to be known and fixed at a value of 0.2.

For the identifiability check of the sought parameters $\mathbf{x}$ the local sensitivities of measurable quantities with respect to model parameters are computed using a calibrated FE model. The sensitivities are shown in Fig. 8, where each bar corresponds to the norm of the displacement field computed using the formula:

$$s_i = \frac{\|\mathbf{u}_i\| - \|\mathbf{u}_{REF}\|}{x_i + \delta x_i - x_i}\frac{x_i}{\|\mathbf{u}_{REF}\|} = \frac{\|\mathbf{u}_i\|/\|\mathbf{u}_{REF}\| - 1}{\delta} \tag{36}$$

where $\mathbf{u}_{REF}$ is a reference displacement field computed using an FE model and feed with a set of parameters shown in Table 4; $\mathbf{u}_i$ is a displacement field that has been computed through perturbation of the parameter x_i by 1% ($\delta = 0.01$). The higher bars in Fig. 8 indicate parameters, which are more likely to be identified through use of DIC measurements.

In order to check the robustness of the proposed identification method, a particular type of numerical test is selected here as a benchmark, namely the pseudo-experimental method. In such an approach, one generates from the numerical FE model feed with known material parameters, the pseudo-experimental data which is later noised and truncated to an assumed testing equipment precision. Using such data, one can be sure of the parameters which have to be identified and so can provide proof that the procedure can converge to the sought parameters. What is known in the literature as 'numerical crime' is avoided here by using a different numerical model for both the identification procedure and for pseudo-experimental generation of data.

Figs. 9 and 10 demonstrate the convergence process for two inverse analyses, each with individual initializations of sought parameters values. Both results present successful characterization of all sought parameters (with the exception of tensile strength σ_t which is not active in such test). The minimum value of the cost function stabilizes after several iterations (7–8 iterations). In the identification procedure

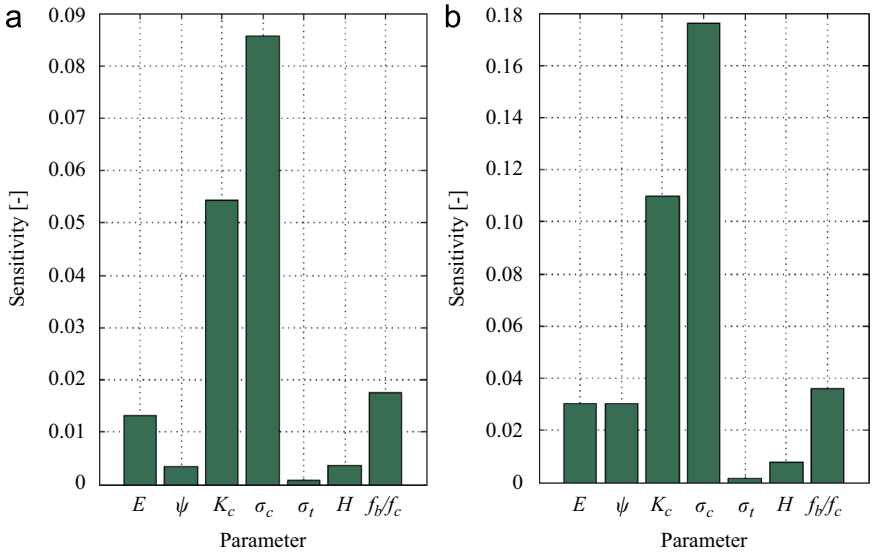

Fig. 8 – Sensitivities of measurable quantities with respect to model parameters in both (a) the *x*- and (b) the *y*-directions.

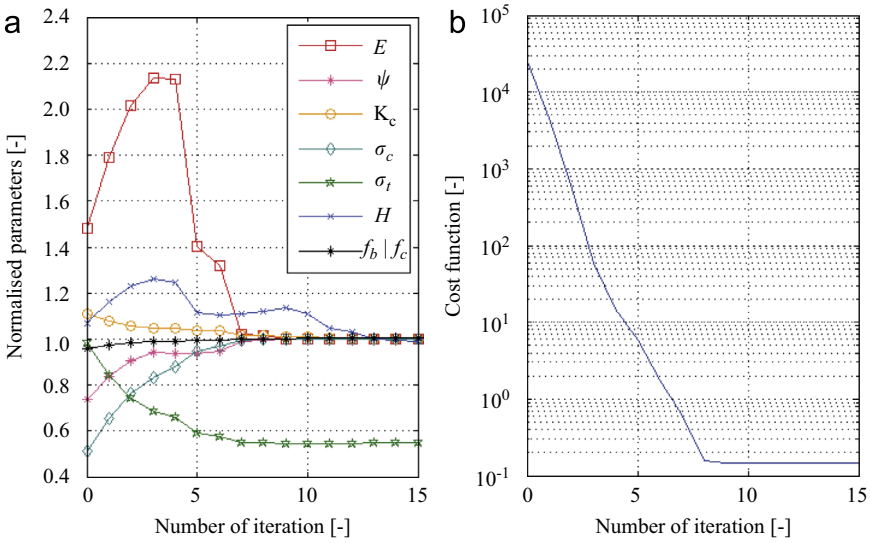

Fig. 9 – Pseudo-experimental inverse procedure results with a random distribution of initial material parameters $x_0^{(1)}$ with accuracy 10 μm, for: (a) convergence of the parameters and (b) the cost function.

presented here, six out of seven normalized parameters (x_i/x_i^{ref}) converge to 1.0, meaning their values are equal to the values of the parameters used to generate the pseudo-experimental data (see Table 4). It should be noted that the illustrated results refer to pseudo-experimental data that has been noised and truncated to an accuracy of 10 μm.

4. Conclusions

Calibration of concrete material with its numerous constitutive parameters usually requires several tests at different level of difficulties and specimen configurations. Here, a simple procedure combining a standard uniaxial test, DIC measurements and inverse analysis highlights a successful characterization of the selected material constants for concrete. By a proper selection of identification tools, namely a fast DIC algorithm, a robust minimization technique and a careful selection of the appropriate constitutive model for a numerical test simulation, one can easily find a set of sought parameters from a single and typical laboratory test.

The Newton–Raphson correlation algorithm surpasses in performance the traditional course-fine algorithm, even if the former is improved by the bicubic interpolation scheme. The TRA that has been presented in this paper already has a wide application in inverse analysis problems (see e.g. [9,10]), its performance shown in this example proves its ability to find fast solutions, which can be obtained even with just a few iterations of highly noised data.

Additional equipment (such as a camera and DIC algorithm) resulting in additional measurements from a single

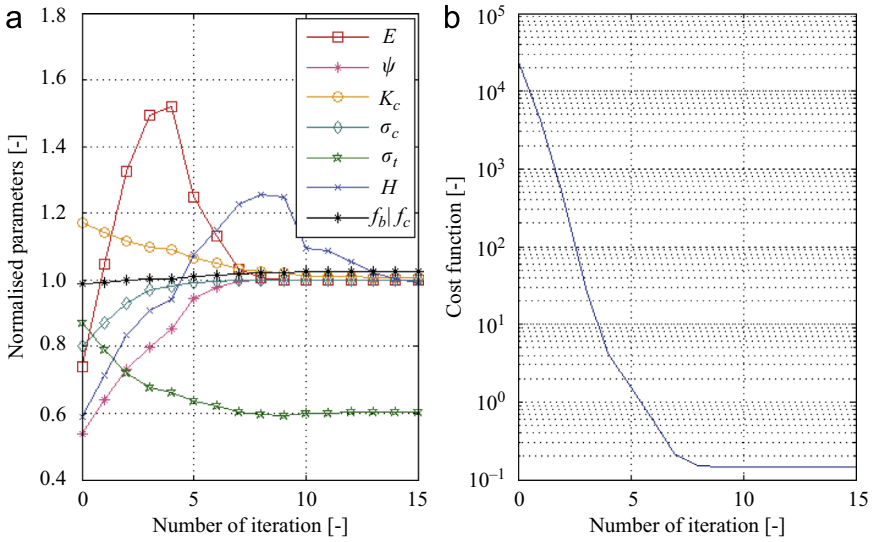

Fig. 10 – Pseudo-experimental inverse procedure results with random distribution of initial material parameters $x_0^{(2)}$ with accuracy 10 μm, for: (a) convergence of the parameters and (b) the cost function.

test, clearly helps to identify more parameters. Such an approach, however, also requires a computer with specialized software for both photograph correlation and numerical simulations. This might be viewed as a limitation especially when tests have to be performed on a routine basis in laboratories. A remedy to the underlined limitation of the presented method could be to preliminarily prepare the models and to simulate the tests on a powerful computer, using a wide range of variations in parameters, which can be later used to build an approximation of the model. Using model reduction techniques (such as artificial neural networks, polynomial approximation, radial basis functions approximation, Gaussian processes, etc.), one can speed up parameter identification (see e.g. [3,9,10]) by several orders of magnitude.

The methodology presented in this paper of identification of concrete parameters from a single test can furthermore be successfully used without heavy computation so long that an approximation of the direct model has been constructed. The numerical model and/or its surrogate require the previously presented combination of DIC measurements together with a rapid correlation algorithm, and efficient experimental and inverse techniques in order to provide a fast and robust characterization of a complex model from a simple test. It is evident from the presented examples that standard testing information (i.e. the force-displacement curve) enhanced with DIC measurement and inverse analysis can be used to successfully calibrate a concrete material model.

REFERENCES

[1] A.J. Abbo, S.W. Sloan, A smooth hyperbolic approximation to the Mohr–Coulomb yield criterion, Computers & Structures 54 (3) (1995) 427–441.

[2] H.A. Bruck, S.R. McNeill, M.A. Sutton, W.H. Peters Jr., Digital image correlation using Newton–Raphson method of partial differential correction, Experimental Mechanics 29 (3) (1989) 261–267.

[3] V. Buljak, Inverse Analyses with Model Reduction: Proper Orthogonal Decomposition in Structural Mechanics, Springer, 2012.

[4] M. Cervera, M. Chiumenti, Mesh objective tensile cracking via a local continuum damage model and a crack tracking technique, Computer Methods in Applied Mechanics and Engineering 196 (2006) 304–320.

[5] A.C.T. Chen, W. F Chen, Constitutive relations for concrete, ASCE Journal of Engineering Mechanics Division 101 (4) (1975) 465–481.

[6] A. Dragon, Z. Mroz, A continuum model for plastic-brittle behaviour of rock and concrete, International Journal of Engineering Science 17 (2) (1979) 121–137.

[7] W. Drucker, D.C. ans Prager, Soil mechanics and plastic analysis or limit design, Quarterly of Applied Mathematics 10 (1952) 157–165.

[8] P.H. Feenstra, R. De Borst, A composite plasticity model for concrete, International Journal of Solids and Structures 33 (1996) 707–730.

[9] T. Garbowski, G. Maier, G. Novati, Diagnosis of concrete dams by flat-jack tests and inverse analyses based on proper orthogonal decomposition, Journal of Mechanics of Materials and Structures 6 (1–4) (2011) 181–202.

[10] T. Garbowski, G. Maier, G. Novati, On calibration of orthotropic elastic-plastic constitutive models for paper foils by biaxial tests and inverse analyses, Structural and Multidisciplinary Optimization 46 (1) (2012) 111–128.

[11] P. Grassl, M. Jirasek, Damage-plastic model for concrete failure, International Journal of Solids and Structures 43 (2006) 7166–7196.

[12] F. Hild, B. Raka, M. Baudequin, S. Roux, F. Cantelaube, Multiscale displacement field measurements of compressed mineral-wool samples by digital image correlation, Applied Optics 41 (32) (2002) 6815–6828.

[13] T. Jankowiak, T. Lodygowski, Identification of parameters of concrete damage plasticity constitutive model, Foundations of Civil and Environmental Engineering 6 (2005) 53–69.

[14] L. Jason, A. Huerta, G. Pijaudier-Cabot, S. Ghavamian, An elastic plastic damage formulation for concrete: application to elementary tests and comparison with an isotropic

damage model, Computer Methods in Applied Mechanics and Engineering 195 (52) (2006) 7077–7092.
[15] J.W. Ju, On energy-based coupled elastoplastic damage theories: constitutive modeling and computational aspects, International Journal of Solids and Structures 25 (7) (1989) 803–833.
[16] J. Lee, G.L. Fenves, Plastic-damage model for cyclic loading of concrete structures, Journal of Engineering Mechanics 124 (8) (1998) 892–900.
[17] J.S. Lee, I.Y. Choi, H.N. Cho, Modeling and detection of damage using smeared crack model, Engineering Structures 26 (2) (2004) 267–278.
[18] T. Li, R. Crouch, A plasticity model for structural concrete, Computers & Structures 88 (2010) 1322–1332.
[19] F.B. Lin, Z.P. Bazant, J.C. Chern, A.H. Marchertas, Concrete model with normality and sequential identification, Computers & Structures 26 (6) (1987) 1011–1025.
[20] J. Lubliner, J. Oliver, S. Oller, E. Oñate, A plastic-damage model for concrete, International Journal of Solids and Structures 25 (3) (1989) 299–326.
[21] B. Luccioni, S. Oller, R. Danesi, Coupled plastic-damaged model, Computer Methods in Applied Mechanics and Engineering 129 (1–2) (1996) 81–89.
[22] MATLAB. version 7.13 (R2011b). The MathWorks Inc., Natick, Massachusetts, 2011.
[23] Ph. Menetrey, K.J. Willam, Triaxial failure criterion for concrete and its generalization, ACI Structural Journal 92 (3) (1995) 311–318.
[24] J. Nocedal, S. Wright, Numerical Optimization, Springer, 2006.
[25] B. Pan, K. Qian, H. Xie, A. Asundi, Two-dimensional digital image correlation for in-plane displacement and strain measurement: a review, Measurement Science and Technology 20 (6) (2009).
[26] H. Park, J.Y. Kim, Plasticity model using multiple failure criteria for concrete in compression, International Journal of Solids and Structures 42 (8) (2005) 2303–2322.
[27] S.W. Park, Q. Xia, M. Zhou, Dynamic behavior of concrete at high strain rates and pressures: II. Numerical simulation, International Journal of Impact Engineering 25 (9) (2001) 887–910.
[28] W.J.M. Rankine, On the stability of loose earth, Philosophical Transactions of the Royal Society of London 147 (1857) 9–27.
[29] L. Resende, J.B. Martin, Formulation of Drucker–Prager cap model, Journal of Engineering Mechanics 111 (1985) 855–881.
[30] M.A. Sutton, J.J. Orteu, H. Schreier, Image Correlation for Shape, Motion and Deformation Measurements, Springer, 2009.
[31] S. Weihe, B. Kroplin, R. De Borst, Classification of smeared crack models based on material and structural properties, International Journal of Solids and Structures 35 (12) (1998) 1289–1308.
[32] J.Y. Wu, J. Li, R. Faria, An energy release rate-based plastic-damage model for concrete, International Journal of Solids and Structures 43 (3–4) (2006) 583–612.
[33] J. Zhang, Z. Zhang, C. Chen, Yield criterion in plastic-damage models for concrete, Acta Mechanica Solida Sinica 23 (3) (2010) 220–230.